

Experimental characterization of fatigue strength in butt welded joint considering the geometry and the effect of cooling rate of the weld

Nelson Arzola¹ and Edgar Hernández²

Research Group in Multidisciplinary Optimal Design, Department of Mechanical and Mechatronics Engineering, National University of Colombia, Cra. 30 No. 45-03 Bogotá D.C., Colombia, Phone (571) 316 5000 Ext. 14 062, Fax (571) 316 5333.

Email: ¹ narzola@unal.edu.co; ² edhernandezl@unal.edu.co

Abstract. In this work the experimental characterization of fatigue strength in butt welded joints considering the geometry and the post-weld cooling cycle was performed. ASTM A-36 structural steel was used as the base metal for the shielded metal arc welding process, with welding electrode E6013. Two experimental factors were established: weld bead geometry and the post-weld cooling rate. Two levels for each factor, the welding reinforcement (1 and 3 mm), and the rate of cooling, slow (quiet air) and fast (immersion in water) are evaluated respectively. For the uniaxial fatigue tests, 8 samples were selected for each treatment for a total of 32 specimens. The mechanical and fractomechanical properties of fusion zone, heat affected zone and base metal in relation to the analysis of failure mechanisms were analysed. The fatigue crack growth rates were estimated based on the counting of microstrations. Furthermore, experimental tests, such as uniaxial tension, microindentation hardness, Charpy impact and metallographic analysis, were made to know the influence of the experimental factors in the fatigue strength. On this research, about the 78.13% of the samples obtained a resistance higher than the recommended one by class FAT 100. The results showed that the geometry of the joint is the factor of greatest influence on fatigue strength for butt welded joints; the greater the weld reinforcement the lower the fatigue strength of the joint. Although it is also important to consider other geometric factors of less impact as it is the weld toe radius and the welding chord width.

Keywords: Butt weld joint; fatigue; crack growth rate; weld reinforcement; rate of cooling.

1. Introduction

The origin of fatigue failure in butt welded joints is caused by different factors, it could be human factor or factors inhered to the process of fabrication employed. The most common imperfections are discontinuities like cracks, undercuts, lack of fusion, porosities and inclusions among others. The fatigue strength in the joint is related to the geometric profile and the coalition between the filler material and the base material. As a result of the thermal cycle experienced during the joint process, there is produced three zones with microstructural differences: the fusion zone (FZ), the heat affected zone (HAZ) and the base metal (BM).



A main evaluation of fatigue strength in the welded joints is thought the initiation process and crack propagation, which depends on the local stress notch in the weld toe and weld root, and the stress intensity factor (SIF) respectively [1]. To predict the fatigue strength from the structures or welded joints it is common to use the S-N curve method, where S is the nominal stress amplitude as a function of N that is the failure number of cycles. Besides, the S-N curve characterizes the limit stress from the notch or the class of detail establish by the British Standard Institution (BSI) [2]. In butt welding joints with a transversal load applied to the weld, the class is between 80-90 according to [3] and C class according to [4], as it is shown in figure 1. Those curves are developed up to two million cycles and are called class FAT.

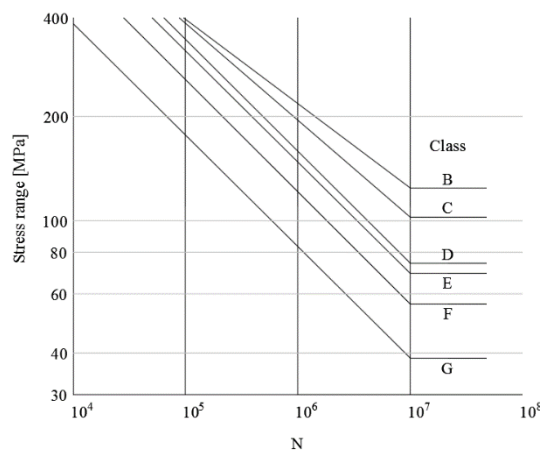


Figure 1. The S-N Curves for the various classes of welded joints [4].

Because the S-N curve is not intended to identify the crack propagation stage, it is necessary to use the empiric relation given by Paris and Erdogan [5]. This expression allows the evaluation of the crack propagation rate (da/dN) as function of the SIF range (ΔK), where C and m are material constant values:

$$\frac{da}{dN} = C(\Delta K)^m \quad (1)$$

In a double logarithm graphic from $\log(da/dN)$ in function of $\log(\Delta K)$ it is possible to obtain three characteristic regions shown in figure 2. The region I, known as the fatigue crack initiation stage, is used to determine the threshold stress intensity range ΔK_{th} for large cracks, although the classification between large and shorts cracks is not clearly established. If a crack is completely in the plastic zone and/or its size related to the propagation direction it's than lower to 0.5 mm it is possible to say that it is a short crack [6]. The region II could be represented by equation (1), which occupies the greater fatigue life percentage, related to regions I and III. In the same way it describes a stable crack propagation stage. Finally, region III presents a sudden increase of the crack propagation rate, giving as a result the final fracture when the fracture toughness of the material is reached.

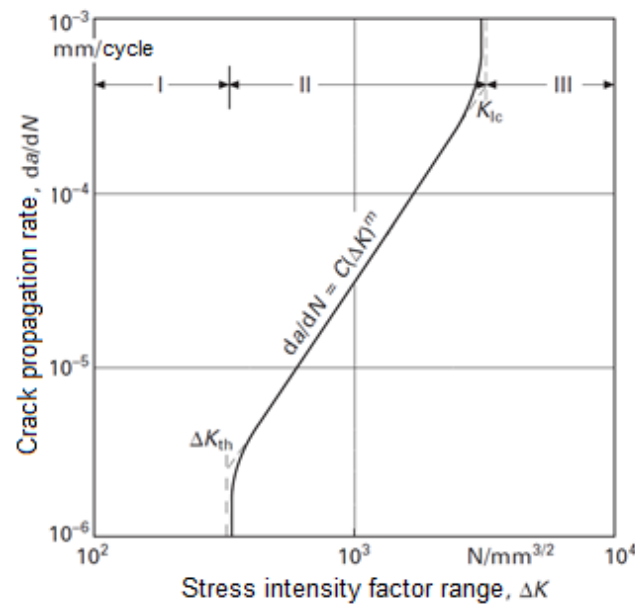


Figure 2. Fatigue crack growth diagram [6].

One of the current methods used to evaluate the fatigue in welding joints is the Fracture Mechanics. Its principal application is the element analysis that contains any type of imperfection, especially elliptic cracks as it is shown in figures 3 and 4. The Fracture Mechanics considers every single stress and its distribution through the thickness of the plate, where the calculation of the crack propagation is governed by the maximum principal stress, because the maximum energy released is presented in the crack propagation perpendicular to the maximum principal stress direction [6].

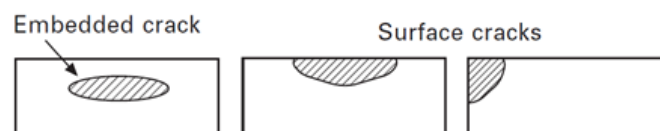


Figure 3. Types of semielliptical cracks [6].

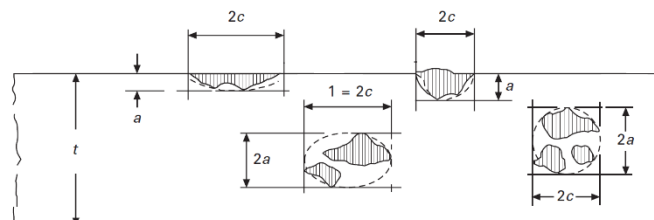


Figure 4. Transfer to NDT into elliptical cracks [6].

In the fracture surface it is common to observe different characteristic scratch that depends on the load type and the environment, among other factors [7]. Two characteristic zones are observed by the uniaxial fatigue on the fracture surface. The first of them is the stable crack propagation which has a smooth or granular texture that can be seen by the human eye. The second zone is called the final fracture because

in this zone the mechanical element is not able to resist the cyclic peak load, and generates the final fracture. The common fractures surfaces marks are shown in figure 5 those marks are related to the mechanical uniaxial fatigue like: river marks, beach marks, ratchet marks, the crack origin and in some cases the striations can be observed through a scanning electron microscope (SEM).

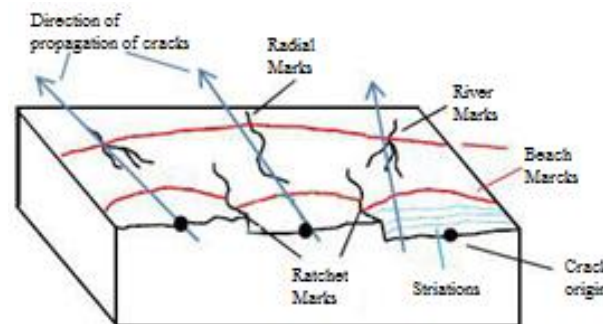


Figure 5. Common marking on fatigue surfaces [6].

The beach marks location determines the fatigue stable crack propagation zone, although it is possible to find them in the fracture surface by stress-corrosion. In the weld joint failure, it is possible to find the crack origin by the beach marks. In that way the striations are fracture surface marks that indicate the crack front shape and size after the fatigue cycle load, however in order to observe them it is necessary to use a SEM. Moreover, the ratchet marks are generated by the interaction of different crack origins, where each one of them produces its own fatigue crack stable propagation zone. Despite this, the different crack fronts can coalesce in a single progressive main crack front as it moves [8].

Different mechanical properties are not constant in weld joints such as yield strength, tensile strength, hardness, fracture toughness, among others. This is caused because of the thermal gradient generated in the fabrication process and the cooling process which has been subjected the welded joint. For that reason, it is necessary to evaluate those properties for the three welded joint zones, the FZ, HAZ and BM, in order to obtain accurate results in terms of welded joint strength [9]. The more common tests used in mechanical characterization for the welded joints are: microindentation hardness [10], uniaxial mechanical stress [11] and Charpy Impact test [12-15], among others. Besides the mentioned tests, the metallographic characterization plays an important role in the welded joint mechanical properties; it allows linking the different microstructural mechanic phases on the joint with its mechanical behavior.

This article describes an experimental study of the fatigue failures on butt welded joints for structural carbon steel ASTM A-36 used in the electric arc welding process with coated electrode E6013. The influence in the geometric joint was evaluated as well as the post weld cooling environment by the uniaxial fatigue tests and the failure mechanism analysis present in the fracture surface. In collateral tests, the mechanical and fractomechanical properties from the welded joints were analyzed in relation with the crack origin and propagation caused by fatigue.

2. Materials and methods

2.1. Experimental design

For the uniaxial fatigue tests, 8 replicas were selected for each treatment accounting for a total of 32 test specimen. Two experimental factors were established: weld bead geometry and the post-weld heat treatment. Two levels for each factor the welding reinforcement (1 and 3 mm), and the rate of cooling, slow (quiet air) and fast (immersion in water) are evaluated, respectively. For the uniaxial tension test three samples were evaluated, as total sampling amount for each treatment, accounting a total of 12 test specimens, and for the Charpy impact test six replicas for each treatment were done, 3 in the (FZ) and

3 in the (HAZ), respectively; additionally 3 more replicas were analyzed for the base metal (BM), thus 27 test specimens were obtained for the late type of test. In order to make easier the data management a codification system was assigned for each test type and cooling medium correspondingly, which is found in table 1 for the uniaxial fatigue test specimens, table 2 for the uniaxial tension test and finally in table 3 for the Charpy Impact samples, respectively.

Table 1. Codification system for the uniaxial fatigue test specimens.

1 th digit	Weld Reinforcement	~1 mm	1
		~3 mm	3
2 nd digit	Cooling Medium	Air	A –
		Water	W –
3 rd digit	Consecutive numbering for replicas		1 – 8

Table 2. Codification system for the uniaxial tension test specimens.

1 th digit	Weld Reinforcement	~1 mm	1
		~3 mm	3
2 nd digit	Cooling Medium	Air	A
		Water	W
3 rd digit	Uniaxial tension		– T –
4 th digit	Consecutive numbering for replicas		1 – 3

Table 3. Codification system for the Charpy-V notch test specimens.

1 th digit	Weld Reinforcement	~1 mm	1
		~3 mm	3
2 nd digit	Cooling Medium	Air	A
		Water	W
3 rd digit	Charpy Impact	– CVN –	
4 th digit	Impact Zone	Fusion Zone	FZ –
		Heat Affected zone	HAZ –
		Metal Base	MB –
5 th digit	Consecutive numbering for replicas		1 – 3

2.2. Materials

The metal base (MB) employed on the welded samples fabrication for the uniaxial fatigue and uniaxial tension, was the rolled carbon structural steel ASTM A-36 with a thickness of 6 mm, while for the impact test a thickness of 12 mm was used. The chemical composition of the material was determined by spark

spectrometry test UV-VIS, results are presented in table 4 and the mechanical properties are shown in table 5.

Table 4. Chemical composition for ASTM A-36 steel, (Wt. %).

C	Si	Mn	P	S
0,202	0,030	0,532	0,028	0,011

Table 5. Mechanical properties for ASTM A-36 steel.

Yield Stress [MPa]	Ultimate Tensile Strength [MPa]	Elongation [%]
262	434	38

2.3. Welding procedure

On the welded joints fabrication as providing material the welding electrode E6013 was employed. The welding direction was performed perpendicular to laminar direction of MB. For welding procedure the plane to top position was utilized with a square joint design following [12], voltage ranging between 15 – 42 V and current between 85 – 140 A (direct current). Approach speed between 2 and 3 mm/s. The applied passes were varied according to the over-thickness width s following: single pass for $s = 1$ mm and two passes for $s = 2$ y 3 mm respectively.

2.4. Uniaxial fatigue test

The test specimen dimensions for the fatigue and uniaxial tension test are shown in figure 6. The same geometry was used for the samples on both tests in order to facilitate their fabrication. However, the AWS B4.0:2007 and ASTM E606 standard were taken into account respectively. Subsequently to post-welding procedure, the final geometry of test specimens was achieved with a waterjet cutting machine to avoid modifications on post-welding treatment. For uniaxial fatigue experimental test a non-standard installation was used. Holding and measuring machine mechanism is supported on two fixed plates where the assembly, for load-cell and sample to be tested, is placed as it is shown in figure 7. Frequency used on uniaxial fatigue test was 4 Hz, peak applied load was 12 kN with a load cycle ratio. $R = 0.05$. A load cycle ratio $R > 0$ in order to guarantee non compressive contact between the crack sides and the information lost concerning its propagation rate is selected.

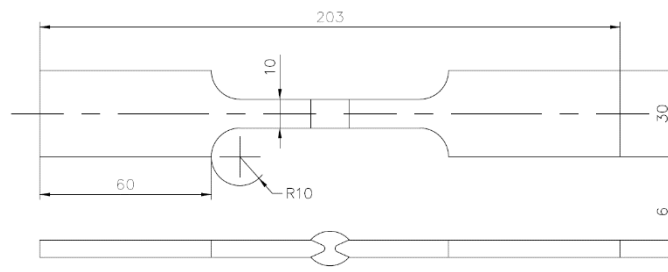


Figure 6. Dimensions for tensile and fatigue test specimens (mm).



Figure 7. Butt welded specimen in the axial fatigue equipment.

2.5. Uniaxial tension test, microindentation hardness test and Charpy V-notch test

The uniaxial tension test were performed following the standard ASTM E8 in a universal test machine Shimadzu UH-500 kNI aiming to obtain the mechanical tension characterization of the studied samples. The hardness test by microindentation were performed in relation with sample thickness (6mm) on three equidistant lines and a third of the sample thickness, employing a durometer LECO M-400-G2 Hardness Tester with a load of 500 gr during 10 s ($HV_{0.5}$). Fabrication of the sample for the energy of impact characterization test, its geometry and percentage of fracture due to shearing were done accordingly the standard ASTM A370 as it is shown in figure 8. The tests were performed at environmental temperature ranging from 19.06 – 19.10°C. A chemical macro attached was performed with Nital at 3% over the welding profile in order to place the notch in the center of zones HAZ and FZ as it is shown in figure 9 following standard ISO 15653.

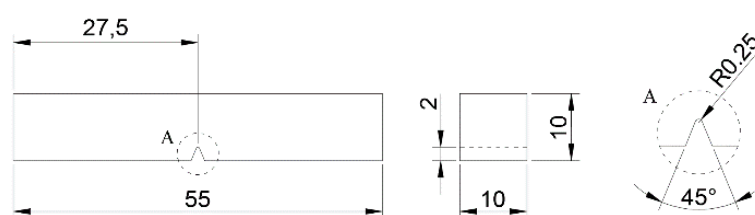


Figure 8. Specimen for impact Charpy V-notch test (mm) following standard ASTM A370.

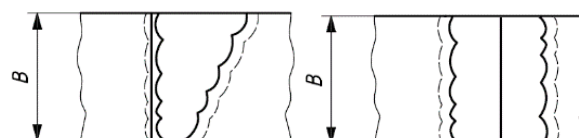


Figure 9. Notch location in HAZ (left) and FZ (right), following standard ISO 15653.

2.6. Microstructure and fractography

Samples used for metallographic test were polished and subsequently attached with Nital at 3%. The microstructural characterization of zones FZ, HAZ and BM was performed by an optical microscope and SEM. Alike the analysis of failures over crack surface was performed on the welded joints in order to identify the crack origin, stable propagation crack zone and its limit. Through observation with stereoscope the stable propagation crack zone to readily use the SEM, which was used for the counting procedure of striations close to initiation and near the end of stable propagation crack zone, as it is described on the study carried out by DeVries et al. [16].

3. Results and discussion

Using as reference FAT 80 and FAT 100 classes in figure 10 the comparison between results for uniaxial fatigue of butt welded joints for the four studied treatments through curve S-N is presented. In this case treatment 3A shows 50% of its results under limit of class FAT 100. Further it is seen that only one sample of treatments 3A and 3W are under limit of class FAT 80; while in majority are the results for samples from treatments 1W and 1A those which represent a greater deviation above limit of class FAT 100. Accordingly with results from figure 10, it is observable the stochastic nature on the fatigue behaviour of butt welded joints. Owing to this, it is necessary to perform a statistic evaluation of the results. Based on [3] a statistic procedure to evaluate surviving probability as function of fatigue capacity ($\log C$), which is obtained through equation (2). Where it is set $m = 3$ for the steels was employed.

$$\log N = \log C - m \cdot \log \Delta \sigma \quad (2)$$

Subsequently the surviving probability in relation to values of $\log(C)$ for 32 analysis samples is obtained, in a normal probability graphic as it is presented in figure 11.

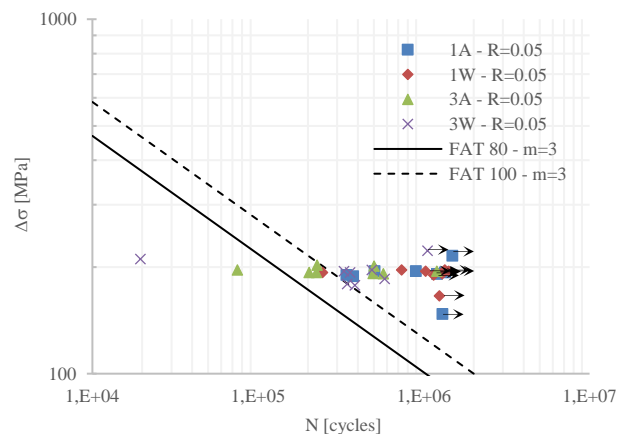


Figure 10. The S-N Curves for treatments of study accord with the classes FAT 80 and FAT 100.

In figure 11 it is possible to identify the behavior of welded samples in comparison with figure 10, even though initially it is necessary to obtain curve S-N to determine the dispersion among analysis information. In figure 11 it is observable that in treatment 1A approximately 63% of the samples are above the 70% of surviving probability, remaining are between 30 and 50% of surviving. In the treatment 1W the 87.5% of the samples are between the 60 and 90% of surviving and remaining in 19%. In treatment 3A the 50% of the samples are between 40 and 80% of surviving and the other 50% of the samples are between 2 and 20% of surviving. Finally in the samples of treatment 3W, the 87.5% of the samples are between 30 and 70% of surviving and remaining in 0.025%. Thus it is possible to affirm

that treatment 1W is the one which has the highest surviving probability in comparison with the other treatments. On the contrary the treatment 3A shows the lowest probability of surviving.

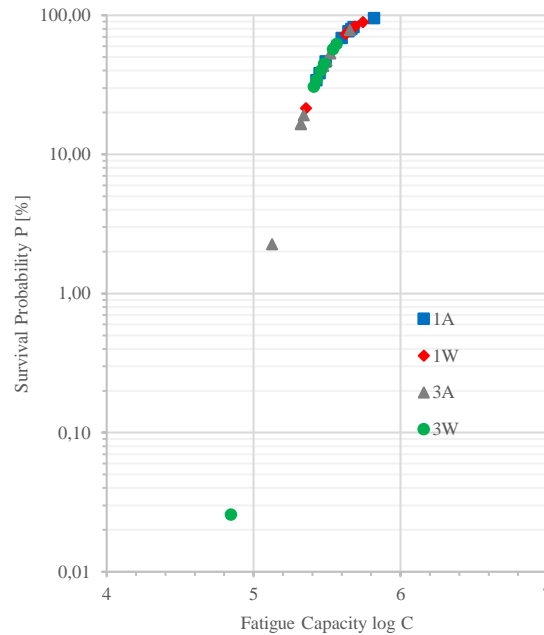


Figure 11. Survival probability for the specimens of fatigue butt welded joint test.

In figure 12 the counting of striations performed on sample 3W-8 is shown. Obtaining two crack propagation rates at beginning of stable zone $\left(\frac{da}{dN}\right)_1$ and close to its end $\left(\frac{da}{dN}\right)_2$. The propagation rates for both locations were estimated by counting and measurement of separation among microstrations, according with [16]. Where C y m are obtained by:

$$C = \frac{\left(\frac{da}{dN}\right)_1}{(\Delta K_{I,1})^m} \quad (3)$$

$$m = \frac{\log\left(\frac{da}{dN}\right)_1 - \log\left(\frac{da}{dN}\right)_2}{\log \Delta K_{I,1} - \log \Delta K_{I,2}} \quad (4)$$

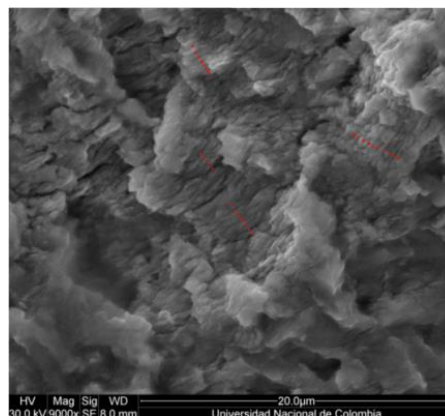
Nevertheless, there are eight replicas for each treatment, in table 6 are shown only the results more representative and with better quality for the constant values C and m . In some of the samples it is not possible to establish the distance among striations, because these are not visible or are confuse among other superficial details.

The propagation curves of cracks for fatigue are shown in figure 13 accordingly with the results obtained in the striation counting from table 6. The curve of sample 1W-8 highlights for the right displacement, which does not mean it has a higher fatigue resistance instead the striation counting was performed for an initial crack size a_1 much higher than used for the other samples. Furthermore it is observed that maximum value for the propagation rate of the cracks is for sample 1A-7 and it is 1.34×10^{-6} [m/cycle], while the sample 1W-8 presents a maximum value of 7.97×10^{-7} [m/cycle] much lower than the previous. This is consistent with experimental results where the life to fatigue for the sample 1A-7 and 1W-8 are 8.98×10^5 and 2.45×10^5 cycles respectively.

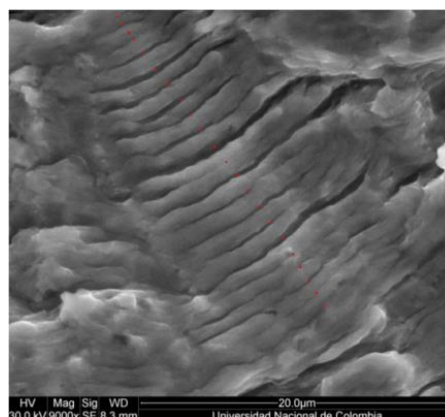
The results of uniaxial tension test for the analysis samples from table 2 are shown in figure 14 and the average of the results for each treatment is presented in table 7. The differences among treatments are not too significant in means of resistance to tension and elastic limit, however. It is important to note that area under the curve for treatment 1W in contrast with treatment 3A present a well-defined difference. This indication allows establishing that treatments 1A and 1W will have a higher resistance to crack propagation than treatments 3A and 3W, as it is observed in results from S-N curve and the surviving probability from figures 10 and 11 respectively. Broadly it is observed that value of tension resistance and elastic limit in butt welded joints increase in relation with properties of BM from table 5. However, the elongation percentage decreases considerably, which leads to a reduction of material ductility of HAZ and FZ.

Table 6. Summary of fatigue striation counting for each treatment.

Specimen	$\left(\frac{da}{dN}\right)_1$ [m/cycle]	$\left(\frac{da}{dN}\right)_2$ [m/cycle]	a_1 [m]	a_2 [m]	$\Delta\sigma$ [MPa]	$\Delta K_{I,1}$ [MPa \sqrt{m}]	$\Delta K_{I,2}$ [MPa \sqrt{m}]	C	m
1A-7	6.28E-7	1.34E-6	9.00E-4	2.45E-3	192	10.23	16.87	6.14E-8	1.51
1W-8	2.34E-7	7.97E-7	2.40E-3	5.29E-3		16.70	24.79	1.40E-8	3.10
3A-4	5.41E-7	1.28E-6	1.09E-3	5.41E-3		11.25	25.07	4.81E-8	1.08
3W-8	3.48E-7	1.14E-6	6.50E-4	4.42E-3		8.69	22.66	4.01E-8	1.24



0 – 0.001 m: 3.48×10^{-7} m/cycle (9000x)



0.004 – 0.0054 m: 1.17×10^{-6} m/cycle (9000x)

Figure 12. Fatigue striation counting close to the crack origin and close to the end of propagation stable stage (stage II), specimen 3W-8.

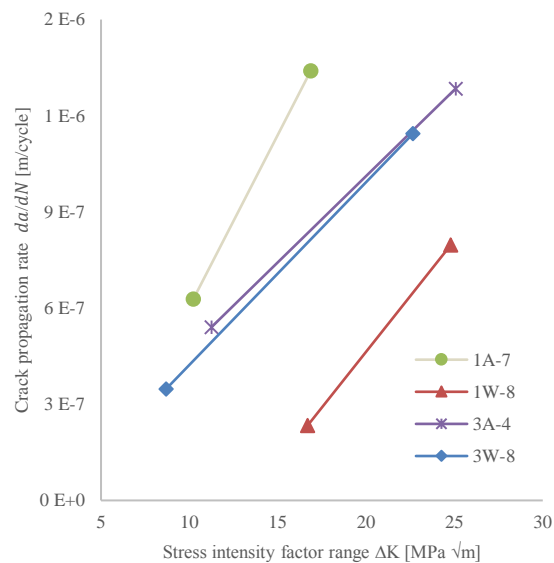


Figure 13. Fatigue crack growth rate in butt joint welds.

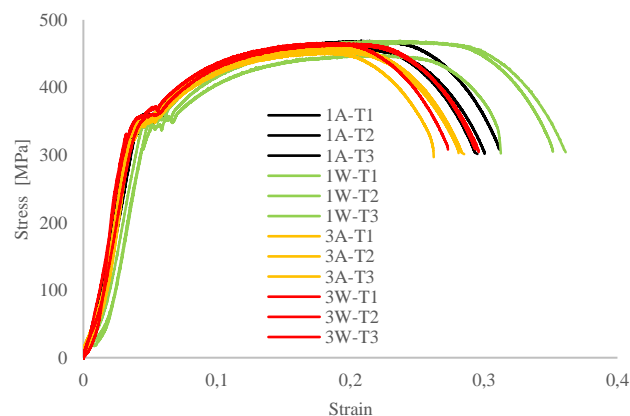


Figure 14. Stress-strain curves of butt welded joints.

Table 7. Results for the mechanical properties obtained by uniaxial tensile test (average values).

Treatment	Ultimate tensile strength [MPa]	Yield stress 0.20% [MPa]	Percent reduction of area [%]	Elongation [%]
1A	462.2	331.6	31.4	19.4
1W	461.3	332.3	32.1	23.3
3A	454.8	321.6	32.1	18.3
3W	465.0	322.2	28.9	19.6

The mean of the results for the Charpy V-notch impact test is shown in table 8. The fracture toughness of the material was estimated indirectly with the Rolfe-Barsom correlation [17]. In figure 15 it is presented a comparison among the percent shear fracture for the highest and lowest percentages obtained

following the standard ASTM A370-14 [13]. Which suggests that percent shear is proportional to material ductility.

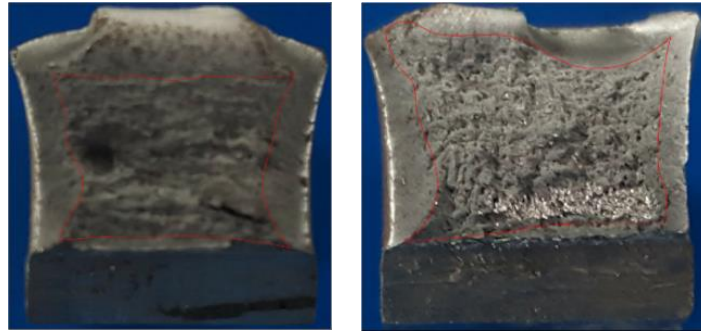


Figure 15. Percent shear fracture 1A-CVN-ZAT (56%) (left); 3W-CVN-ZF (21%) (right).

In relation with cooling cycle it is possible to affirm that a fast cooling rate produces a reduction in the final grain size, thus increasing the material hardness. Moreover, when the welded joint is fast cooled in water immediately after applying the welding chord, a quench is produced due to the fast cooling rate of the welding chord; subsequently if a new welding pass is applied, a tempering and a reduction of the grain size in nears of the late welding chord are produced. In figure 16 it is shown a scheme about grain refinement as a result of multiple passes of welding in a butt welded joint with base on [18]. The columnar microstructure domains in the zone FZ, in interface FZ-HAZ a coarse grain is present, in central zone of HAZ there is a fine grain size; and finally in the interface HAZ-BM it is present a partial refinement.

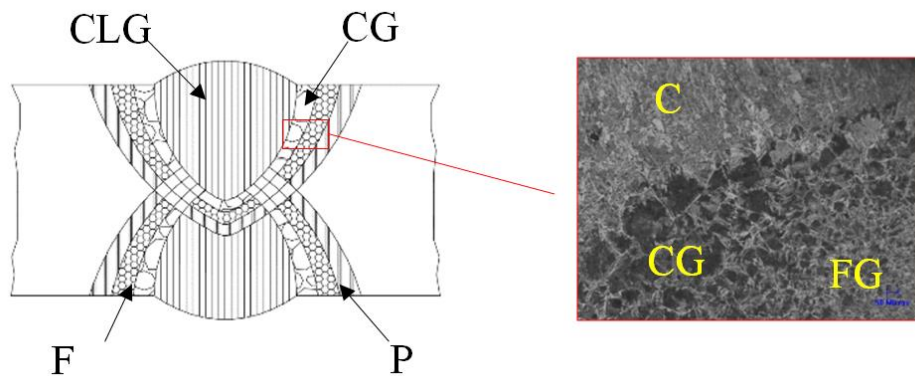


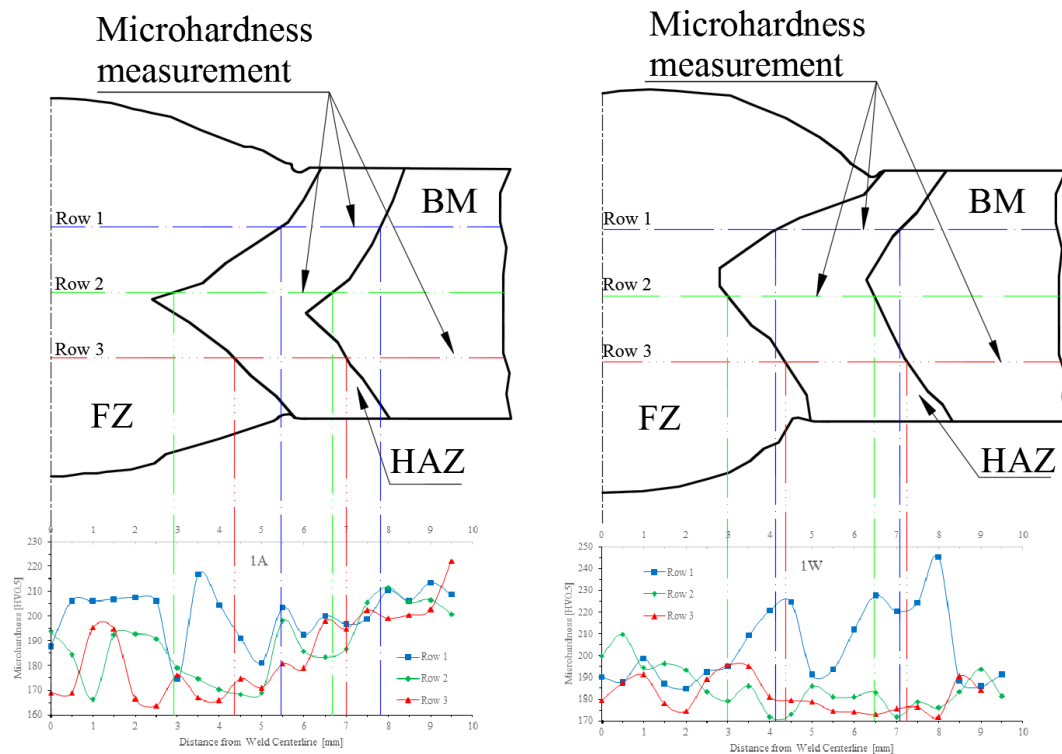
Figure 16. Scheme of grain refinement product of multi-pass welds in a butt welded joint. CLG (columnar grain); CG (coarse grain); FG (fine grain) and RP (partial refinement) [18].

The results obtained from microindentation hardness testing are shown in figure 17, for the 4 studied treatments. The presented profiles are the real ones. These were obtained by means of digitalization of macro structure image and later processing on Academic suite of AutoCAD. A strong tendency to present softness for zone HAZ is presented in these results, owing to the fine grain size as it is shown in figure 16. Though, in samples 1W and 3W this behavior is present in a more pronounced way. Although in figure 17 (superior and inferior image respectively) the hardness increase is observed on rows 1 and 3 for the samples 1W and 3W respectively, the hardness value increases for sample 1W on the interfaces FZ-HAZ and HAZ-BM, while in sample 3W that happens on the interfaces TAZ-BM. The possible

reasons for the previous behavior could be attributed to fast cooling rate and number of welding applied passes, thus generating microstructural variations in size and shape of the grain as it is appreciable in figure 16.

Table 8. Results of impact energy tests CVN (average values).

Treatment	CVN [J]	K_{Ic} [MPa \sqrt{m}]	Shear fracture [%]	Treatment	CVN [J]	K_{Ic} [MPa \sqrt{m}]	Shear fracture [%]
1A-CVN-ZF	100.29	163.33	33	1A-CVN-ZAT	157.04	157.42	56
1W-CVN-ZF	81.17	146.17	33	1W-CVN-ZAT	138.67	147.77	40
3A-CVN-ZF	75.97	141.15	21	3A-CVN-ZAT	125.98	140.73	45
3W-CVN-ZF	66.91	131.94	21	3W-CVN-ZAT	187.01	172.01	31
MB	204.63	180.03	27				



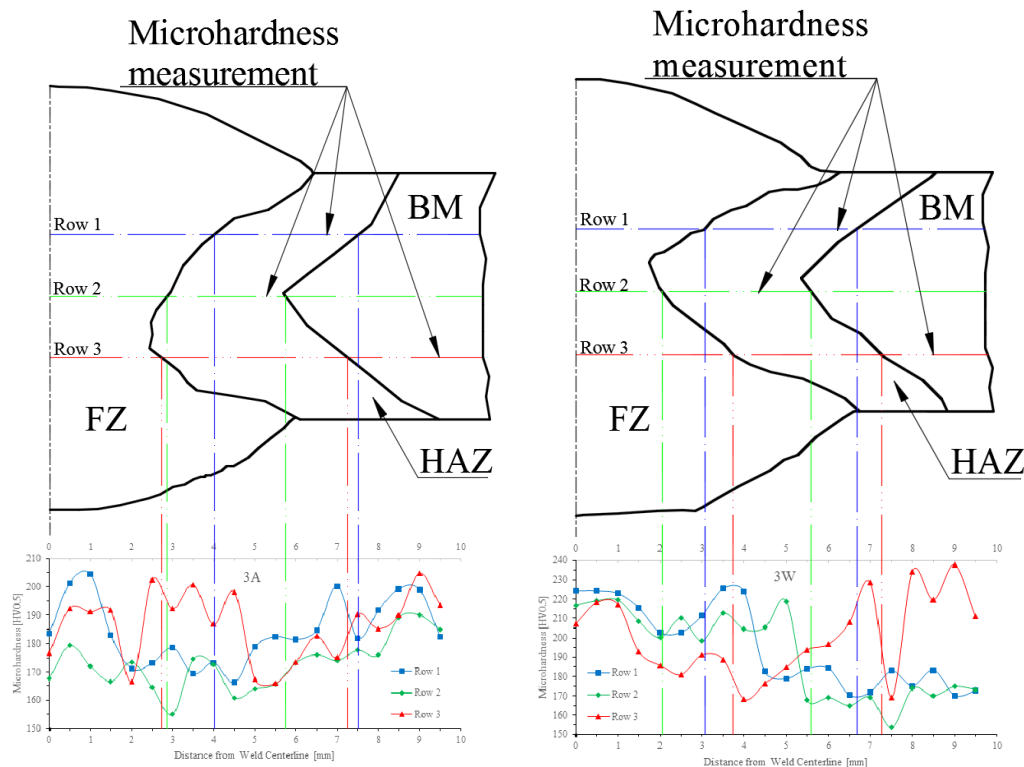


Figure 17. Microindentation hardness profile, specimen 1A (upper left); specimen 1W (upper right); specimen 3A (lower left); specimen 3W (lower right).

For microstructural evaluation of zones FZ, HAZ and BM, the phase diagram Fe-Fe₃C was used as it is shown in figure 18. This method allowed to establish a first correlation between cooling cycle, carbon percentage in the material from table 4 and the microstructural phases present in the different zones of welded joints [19]. Due to the maximum reached temperature and the size of welding pool on process SMAW, it is common to find a columnar ferritic microstructure or an epitaxial growth of the grains in the zone FZ (see figure 18 upper right image). The last is generated by the atomic disposition of liquid metal in relation with the crystallographic orientation of BM [20]. Although when several welding passes are made on zone FZ a grain refinement is produced on the interface of each welding pass [21]. At the limit between zones FZ and HAZ a partial melted zones might be formed as a result of thermal gradient on the material. On this zone a coarse grain size predominates (see figure 18 central left image), where the increase of the grain size decrease the material ductility besides increases the cracking susceptibility due to liquefaction. In figure 18 central right image, the microstructure of zone HAZ is shown. That region clearly contains the microstructural phase ferrite and perlite, bright and dark regions respectively. Where a microstructure with grain size particularly refined, which implies as a consequence a higher ductility. In some cases it is possible to find austenite due to perlite transformation when exceeding 727 °C. However, the austenite in majority decomposes into fine grains of perlite and ferrite. The BM zone figure 18 bottom right image has a microstructure with homogenous ferrite grains and perlite colonies at the ferrite grain limits.

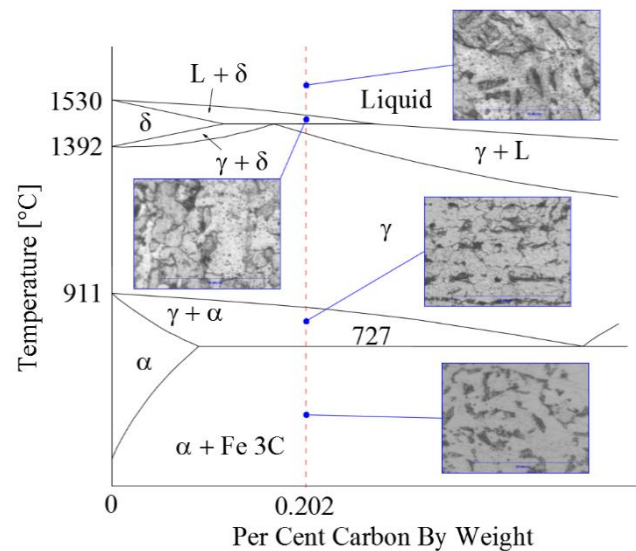


Figure 18. Phase diagram Fe – Fe₃C based on the treatment 1A.

Furthermore of considering the chemical composition of material, it is necessary to evaluate the quenching rate to establish the result of transformations on the zone HAZ. In figure 19 it is shown a scheme of transformations by continuous quenching of steels [19]. Dotted line with double dot (left) defines a fast cooling and the obtainment of a martensitic structure (treatments 1W and 3W) and the dotted line with single dot (right) defines a slow cooling with possible austenitic, ferritic and/or perlitic structures (treatments 1A and 3A).

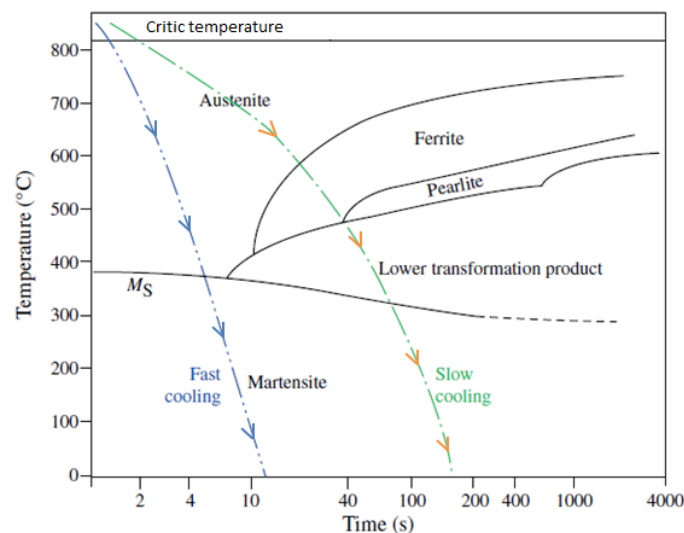


Figure 19. Continuous cooling transformation diagram for steels [19].

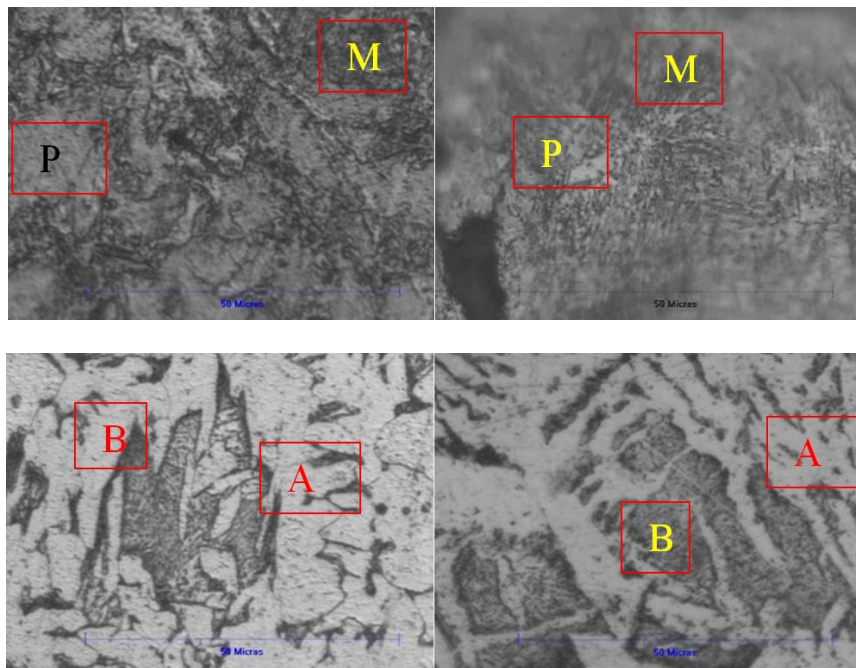


Figure 20. Microstructural phases of ZF-HAZ interface at the weld toe (2000x).

In consistency with the obtained results from uniaxial fatigue test for the failed samples, it was possible to observe that at the crack initiation occurred at the weld toe, mainly on the interface FZ-HAZ, consequently it was decided to analyze the microstructure present in that zone in order to relate the fatigue crack initiation and the microstructure influence. In figure 20 the results of interface analysis are shown for interface FZ-HAZ. Where it is observed the presence of martensitic microstructure (M) and polygonal ferrite (PF) of fine grain in samples 1W and 3W (figure 20 upper left and right images). This is consistent with a fast cooling rate, where pre-eutectoid ferrite disappears and the austenite grains are transformed into acicular structures as: martensite or inferior bainite or a mixture of those [22]. These micro structures have an elevated hardness although a low ductility too, thus favoring the crack propagation due to fatigue and a lower critical crack size, owing to a low fracture toughness to material as it is observed in table 8 when comparing values of the zone FZ and zone HAZ. This agrees with the results shown in figure 10 for the treatment 3W where this treatment exposes the lowest fatigue resistance compared with others. Nevertheless, the treatment 1W, according with results from figure 10 is among the highest resistance values. Which allows concluding that geometric factor of over-thickness has a greater influence on the fatigue resistance than microstructure resulting from cooling cycle, for each of the studied treatments. However, it is important too to consider the amount of welding passes applied in the joint owing to the microstructural variations that might produce. On the other side, for treatments 1A and 3A secondary structures were obtained such as Bainite (B) and acicular Ferrite (AF) (see figure 20 bottom images), as a result of slow cooling rates. Likewise the grain size is much smaller than that obtained in samples 1W and 3W.

Finally, in figure 21, comparison between samples 1A-7 and 3A-5 is carried out in terms of appearance of the failure zone due to fatigue. It is observed that sample 1A-7 presents a single visible crack origin owing to the radial marks point toward a single direction, in opposition the sample 3A-5 contains three dots which indicate the crack origin of superficial semielliptical kind, based on figure 4. In sample 3A-5 (right) it is observed clearly how the three crack fronts, as crack propagation moves along, tend to convert into a single crack front, while in sample 1A-7 (left) the only crack front present propagates more or less in a concentric way around its origin. The bigger the size of stable growth zone

of cracks on the surface of fracture for a same load cycle, it means a higher tolerance to damage of welded joint.

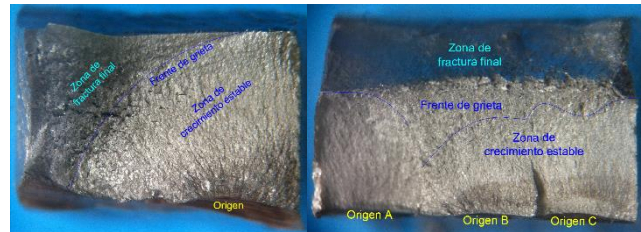


Figure 21. Fatigue fracture surfaces. Specimen 1A-7, $N_f = 8.98 \cdot 10^5$ cycles (left) and specimen 3A-5, $N_f = 0.75 \cdot 10^5$ cycles (right).

4. Conclusions

According with the results obtained experimentally on this research, it is possible affirm that: The fatigue resistance in butt welded joints is strongly influenced by the weld joint geometry, specifically the height of reinforcement weld (s), although it is also important to consider other geometric factors of less impact as it is the weld toe radius to plate, the welding chord width, and material thickness among others.

On this research 93.75% of the samples presented a fatigue resistance superior to the one of class FAT 90, while about the 78.13% of the samples obtained a resistance higher than the recommended one by class FAT 100. If a more conservative approach is preferred, with class FAT 100 a higher security factor will be obtained that counteracts the variability typical of the fatigue behaviour in the welded joints.

The fatigue striation counting allows estimating and validating the fatigue crack growth rate. However, in some cases owing to the post-welding procedure it was not possible, because the zone of crack propagation for fatigue was not ductile enough to generate characteristic marks of striations.

In consistency with welding procedure and post-welding procedure the experimental test as the uniaxial tension, Charpy impact, microindentation and the metallographic observation. Allowed to characterize the mechanical properties of butt welded joints in relation with base metal, where it was clearly observed that the cooling cycle and the amount of passes influence the material ductility and thus the fracture toughness of the material too

In agreement with experimental results, it was found that crack front on the failure surface for fatigue presented an approximated semielliptical shape. This allows establishing in an easier way the numeric modelling for butt welded joints, in order to establish correlations between experimental results and theoretical calculations. On the other hand, it is highlighted the importance of performing additional studies where the nucleation stage and initiation of cracks for fatigue are examined, for that the microstructural phases and the size of the microstructures are more relevant in comparison with the stage of stable propagation of cracks.

References

- [1] Radaj D, 1990 Design and analysis of fatigue resistant welded structures. Abington Publishing.
- [2] BS7608, 2014 Guide to fatigue design and assessment of steel products, BCI Standards Publication.
- [3] Hobbacher A F, 2016 Recommendations for fatigue design of welded joints and components. Cham: Springer International Publishing.
- [4] Schijve J, 2001 Fatigue of structures and materials. Dordrecht; Boston MA: Kluwer Academic.
- [5] Paris P and Erdogan F, 1963 A critical analysis of crack propagation laws, *J. Basic Eng.*, **85**, no. 4, p. 528.
- [6] Hobbacher A, 2011 The use of fracture mechanics in the fatigue analysis of welded joints,

- Fracture and Fatigue of Welded Joints and Structures*, pp 91–112.
- [7] Espejo E and Hernandez E, 2002 Mecánica de fractura y análisis de falla, Colección Universidad Nacional de Colombia
 - [8] Davis J R, 1998 *Metals handbook Desk Edition*. ASM International.
 - [9] Belen’kii D M, Beskopyl’nyi A N, Vernezi N L, and Shamraev L G, 1997 Determination of the strength of butt welded joints, *Weld. Int. J.*, **11**, no. 8, pp 642–645.
 - [10] ASTM E384-16, 2016 Standard test method for microindentation hardness of materials.
 - [11] Standard test methods for tension testing of metallic materials. 2012 West Conshohocken PA: ASTM International.
 - [12] Structural Welding Code Steel 2015 Steel 23rd Edition Supersedes AWS D1.1/D1.1M:2010.
 - [13] ASTM A370-16 2016, Standard test methods and definitions for mechanical testing of steel products.
 - [14] ISO 15653 2010 Metallic materials–Method of test for the determination of quasistatic fracture toughness of welds, *International Standards Organisation*.
 - [15] Potter J and McHenry H 1990 Fatigue and Fracture Testing of Weldments. 100 Barr Harbor Drive, PO Box C700, West Conshohocken, PA 19428-2959: ASTM International.
 - [16] DeVries P, 2010 Counting on Fatigue: Striations and Their Measure, *J. Fail. Anal. Prev.*, **10**, no. 2, pp 120–137.
 - [17] Barsom J and Rolfe S, 1970 Correlations between K_{Ic} and charpy v-notch test results in the transition-temperature range, 100 Barr Harbor Drive, PO Box C700, West Conshohocken, PA 19428-2959: ASTM International, pp 281–281–22.
 - [18] Boukharouba T, Elboujdaini M, and Pluvillage G 2009 Damage and Fracture Mechanics. Dordrecht: Springer Netherlands.
 - [19] Lippold J C, 2015 Welding metallurgy and weldability, *John Wiley & Sons, Inc.* DOI: 10.1002/9781118960332.ch1
 - [20] Kou S, 2002 Welding metallurgy, *John Wiley & Sons, Inc.* DOI: 10.1002/0471434027
 - [21] Kerr H, 1976 A review of factors affecting toughness in welded steels,” *Int. J. Press. Vessel. Pip.*, **4**, no. 2, pp 119–141.
 - [22] Lancaster J F, 1980 Carbon and ferritic-alloy steels, in *Metallurgy of Welding*, Dordrecht: Springer Netherlands, pp 110–177.